Bending and Buckling of Internally-Pressurized Steel Lined Pipes

Bending and Buckling of Internally-Pressurized Steel Lined Pipes

Ilias Gavriilidis[a] and Spyros A. Karamanos*[a,b]

[a] *School of Engineering, Institute for Infrastructure and Environment, The University of Edinburgh, Scotland, UK*
[b] *Department of Mechanical Engineering, University of Thessaly, Volos, Greece*

ABSTRACT

During offshore installation, steel lined pipes are subjected to severe plastic bending, resulting in detachment of the thin-walled liner pipe from the outer pipe and eventually, the formation of local buckling in the form of short-wave wrinkles that menace the structural integrity of the pipeline. The paper focuses on the mechanical behaviour of mechanically lined pipes subjected to monotonic bending, considering for the presence of low and moderate levels of internal pressure, aimed at preventing or delaying wrinkle formation, and improving structural performance. The problem is solved numerically, accounting for geometric non-linearities, local buckling phenomena and elastic-plastic material behaviour for both the liner and the outer pipe. Two types of lined pipes are examined, with and without mechanical bonding between liner and outer pipe referred to as tight-fit and snug-fit lined pipe, respectively. The results demonstrate that the bending performance of lined pipes, under low or moderate internal pressure levels, is significantly improved. The influence of initial geometric imperfections on liner pipe buckling is also examined, showing the imperfection sensitivity of bi-material pipe bending behaviour.

*Corresponding author: E-mail address: spyros.karamanos@ed.ac.uk

1 INTRODUCTION

Steel pipelines, used for oil and gas transmission, are exposed to several corrosive pollutants, such as hydrogen sulphide or chlorides, and water. In order to ensure the structural integrity of the pipeline against corrosion, instead of producing pipelines from stainless steel or nickel alloy, an effective solution to this challenge is a double-wall pipe, called "lined pipe" or "bi-material pipe" (Figure 1). The lined pipe consists of a low-alloy carbon steel outer pipe and a thin-walled pipe from a corrosion resistant alloy material, which is fitted into the thick-walled outer with a specific manufacturing process. The process depends on the manufacturer and ends up in a bi-material pipe.

During offshore installation, the pipeline is subjected to severe bending, so that significant stresses and strains are developed in the pipeline wall, associated with cross-sectional ovalization, which may cause failure of the liner in the form of local buckling. During the last few decades, significant research has been conducted and designing analysis tools are developed, in order to describe the mechanical behaviour of single-walled pipes under bending combined with internal or external pressure (Corona and Kyriakides, 1988; Karamanos and Tassoulas, 1991; Netto and Estefen, 1994). These tools can be used to ensure the structural stability of the thick-walled outer pipe and are summarized in the book by Kyriakides and Corona (2007). Nevertheless, during bending loading, the thin-walled liner pipe is bent together with the outer pipe, detaches from the outer pipe and may buckle in the form of short-wave wrinkles on its wall, while the outer pipe is still structurally stable. These wrinkles are an impediment to the internal flow, might block pipeline pigging equipment, and, under repeated loading, could lead to fatigue cracks because of local stress concentrations (Dama *et al.*, 2007).

Extensive experimental work has been conducted at TU Delft by Focke (2007), investigating the mechanical behaviour of lined pipes in offshore applications, installed by the reeling method. The specimens had outer pipes made of X65 steel with nominal diameter equal to 12.75 *in*, lined with 3 *mm*-thick 316L stainless steel pipes. The liner was fitted into the carbon steel outer pipe resulting in two types of lined pipes, (a) a pipe with zero pre-stress, referred to as "SFP" (snug-fit pipe) and (b) a pipe with mechanical bonding between both pipes, called "TFP" (tight-fit pipe), where the liner

pipe is in hoop compression due to confinement by the outer through a thermo-hydraulic manufacturing process, as described in detail by Focke (2007). Numerical results on these pipes have been presented by Hilberink *et al.* (2010*a*,*b*) continuing the work by Focke (2007) and focusing on liner wrinkling of "snug-fit" pipes (stress-free liner, in contact with outer pipe) and "tight-fit" pipes, under axial compression. In subsequent publications, the influence of friction and mechanical bonding of lined piped have been investigated, comparing also the results with experimental data from four-point bending tests (Hilberink *et al.*, 2011; Hilberink, 2011).

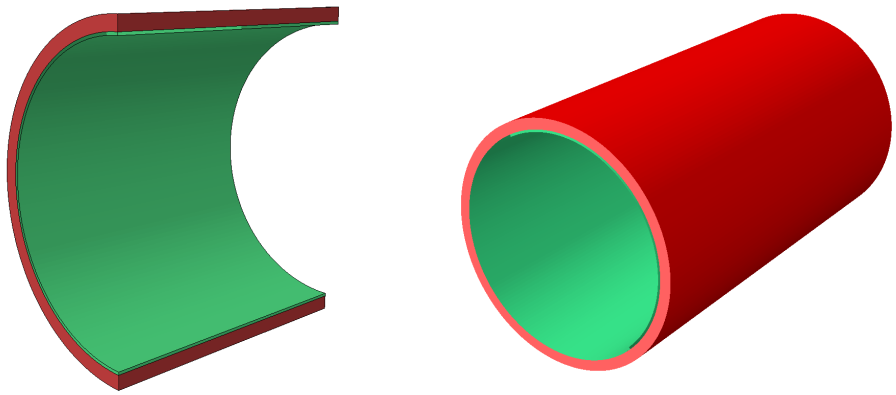

(a) (b)

Figure 1: Visualization of a lined pipe.

Tkaczyk *et al.* (2011) conducted experimental testing for 6.625-*inch* and 12.75-*inch* diameter lined pipes, using the bending facilities of Heriot Watt University, together with numerical analysis, to understand the liner wrinkling process. Subsequently, Tkaczyk and Pepin (2014) presented a patent that proposes analytical expressions for the minimum thickness of the liner pipe, required for reeling installation in the absence of internal pressure. An in-depth numerical investigation of liner pipe buckling has been presented by Vasilikis and Karamanos (2012), simulating the structural behaviour of steel lined pipes subjected to bending. In that work, the wrinkling mechanism of liner pipe has been thoroughly investigated; the detachment between the liner and the outer pipe was detected and two sequential bifurcations were identified. Furthermore, imperfect lined pipes were analyzed, and the results were compared successfully with corresponding experiments. Fur-

ther numerical results on the localized buckling of steel lined pipes during bending have also been presented in a subsequent publication of the authors (Vasilikis and Karamanos, 2013). Numerical results on steel lined pipes under monotonic bending have also been presented by Yuan and Kyriakides (2014*a*,*b*). The mechanical behaviour of liner pipe at girth weld region was also investigated by Yuan and Kyriakides (2015), considering the influence of geometric and material discontinuities on the structural integrity.

The results from the above publications refer mainly to non-pressurized lined pipes. On the other hand, bending of internally-pressurized lined pipes has received much less attention. Full-scale experiments, reported by Toguyeni *et al.* (2012) and Sriskandarajah *et al.* (2013), investigated liner wrinkling under bending in the presence of internal pressure, in an attempt to prevent wrinkle formation. In those tests the level of pressure was 50% of nominal yield pressure. Furthermore, numerical results on the bending response of internally-pressurized lined pipes have been presented by Yuan and Kyriakides (2014*a*,*b*, 2015), showing a delay of liner wrinkling and buckling with respect to the non-pressurized case. Recently, a series of patents were developed (Endal *et al.*, 2012; Mair *et al.*, 2013; Howard and Hoss, 2016), describing the welding process and the spooling of the lined pipe onto the drum, in the presence of relatively high levels of internal pressure (30 *bar*), in order to avoid the separation of the liner from the outer pipe, and proposing alternative ways for reeling installation.

The present paper is motivated by reeling of lined pipes, and focuses on the structural behaviour of lined pipes subjected to monotonic bending in the presence of low and moderate levels of internal pressure. Advanced finite element tools are used to simulate thin-walled liner deformation, including wrinkling and post-buckling behaviour. Numerical results are presented for the "snug-fit" pipe (SFP) and the "tight-fit" pipe (TFP), which account for the hoop compressive pre-stress due to the manufacturing process. The results are presented for several levels of internal pressure and compared with corresponding results from non-pressurized pipes, using ovalization analysis (two-dimensional), as well as three-dimensional analysis models. In addition, a parametric study on the influence of initial wrinkles on the liner is conducted on both types of lined pipes, in an attempt to investigate the imperfection sensitivity of those bi-material pipes.

2 NUMERICAL MODELING

The mechanical behaviour of lined pipes subjected to bending is analysed numerically using non-linear finite element tools. The numerical simulations were conducted using general-purpose finite element program ABAQUS (Hibbitt *et al.*, 2016). The analysis considers non-linear geometry in the description of the liner and the outer pipe, whereas, the materials of the liner and the outer pipe are both considered elastic-plastic through a J_2 (von Mises) flow plasticity model with isotropic hardening, calibrated through uniaxial stress-strain curves from coupon tests, reported in previous publications (Vasilikis and Karamanos, 2012, 2013).

The finite element model is three-dimensional, considering a lined pipe segment of appropriate length L. Based on symmetry of geometry and deformation with respect to the plane of bending, a symmetric model with respect to the y-z-plane is considered, as shown in Figure 2, analysing half of the pipe cross-section. In addition, x-y-plane symmetry of the model is assumed in the $z = 0$ plane allowing only for in-plane motion on the corresponding nodes, while in the $z = L$ plane (as shown in Figure 2), a reference node, in which the rotation is applied, is coupled with the corresponding nodes of the lined pipe cross-section, so that these nodes are allowed to slide on the rotated plane.

The liner pipe is modelled with four-node reduced-integration shell elements (S4R), whereas the outer pipe is modelled using twenty-node reduced-integration brick (solid) elements (C3D20R). As shown in Figures 2a and 2c, the half cross-section of the outer pipe contains 50 elements, while 100 elements are employed around the half-circumference of the liner (as shown in Figures 2b and 2d). This number of elements was found adequate in order to achieve convergence and accuracy of the numerical results based on previous results (Vasilikis and Karamanos, 2012, 2013). Furthermore, contact conditions are imposed between the two pipes and their interface is considered frictionless, an assumption also used in previous works (Vasilikis and Karamanos, 2012, 2013; Yuan and Kyriakides, 2014*a*,*b*, 2015).

The length of the lined pipe model and the number of elements in each pipe depends on the type of simulation to be performed. For ovalization analysis and buckling analysis the corresponding length is described in sections 3.1 and 3.2, respectively, in more detail. To perform ovalization bending analysis of lined pipe, a small-length pipe segment is assumed, which

consists of four and two elements of liner and outer pipe respectively, in the longitudinal direction as shown in Figures 2a and 2b. Considering this small-length segment, wall wrinkling phenomena are excluded, focusing on cross-section ovalization and liner detachment. On the other hand, in order to simulate liner wrinkling, during bending loading, and the corresponding imperfection sensitivity, a longer model is necessary, consisting of two hundred elements for the liner pipe and one hundred elements for the outer pipe, in z-direction as shown in Figures 2c, 2d. This segment has been found necessary for simulating liner wrinkling and will be further discussed in section 3.2.

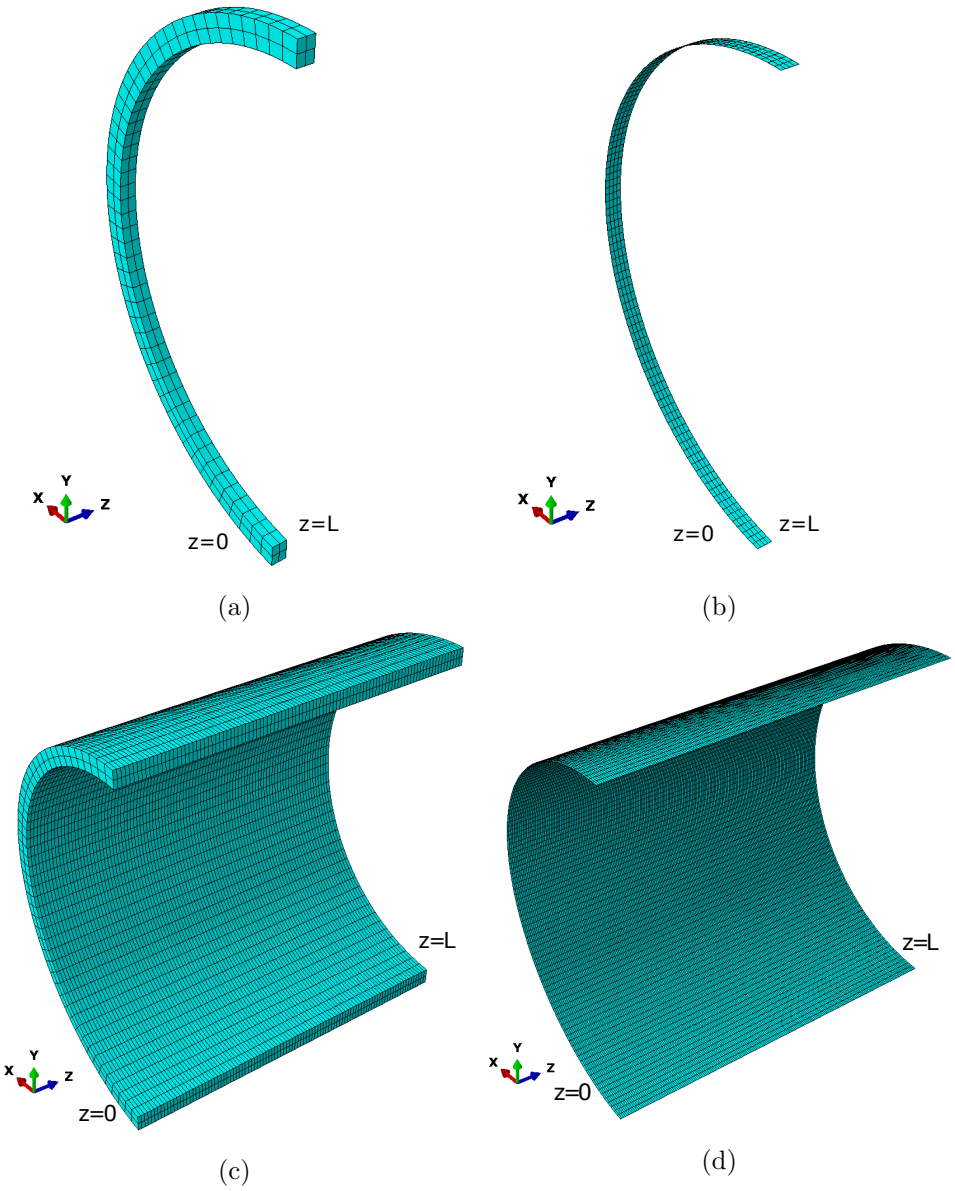

Figure 2: Ovalization analysis model [(a) outer pipe, (b) liner pipe] and buckling analysis model [(c) outer pipe, (d) liner pipe].

3 NUMERICAL RESULTS

A lined pipe, typical for offshore pipeline applications, is considered, similar to a lined pipe examined by Focke (2007). It consists of a thick-walled outer pipe, made from X65 steel material and a stainless steel 316L

liner pipe. The outside diameter (D_o) and thickness (t_o) of the outer pipe are 325 *mm* (12.75 *in*) and 14.3 *mm* (0.56 *in*) respectively, while the liner diameter (D_l) and thickness (t_l) are 296.4 *mm* (11.67 *in*) and 3 *mm* (0.12 in) respectively. The stress-strain curve of the outer pipe material is shown in Figure 3, with Young modulus $E_o = 210,000$ *MPa*, Poisson's ratio $\nu = 0.3$ and yield stress $\sigma_{y,o} = 566$ *MPa*. The corresponding stress-strain curve of the liner pipe material is also shown in Figure 3, with parameters $E_l = 193,000$ *MPa*, $\nu = 0.3$, proportional limit $\sigma_{pr} = 250$ *MPa* at 0.13% and yield stress $\sigma_{y,l} = 298$ *MPa* corresponding to 0.2% residual plastic strain. In section 3.1, an ovalization analysis is performed, considering only cross-sectional deformation, assumed constant along the pipe. In sections 3.2 and 3.3 three-dimensional analysis is conducted, including local buckling effects. In particular, section 3.2 refers to bending of imperfection-free pipes, whereas the effects of initial imperfections are examined in section 3.3.

Following the terminology used by Focke (2007), in the case of TF Pipes, an initial compressive hoop stress of magnitude 200 *MPa* (67.1% of the liner yield stress) is applied on the liner pipe, followed by an unloading step, resulting in residual compressive hoop stress σ_{res} for the liner pipe equal to 166 *MPa*. This is a simple and efficient procedure to account for the manufacturing process, also used by Vasilikis and Karamanos (2012). However, it does not account for the effects of manufacturing on the material properties of the liner. Internal pressure P_{in} is applied, up to 10% of the liner pipe yield pressure ($P_y = 2\sigma_{y,l}t_l/d_{m,l}$, where $d_{m,l}$ is the mean diameter of the liner pipe), and the pressure load parameter $p = P_{in}/P_y$ is introduced. In this case, the maximum internal pressure level corresponds to 6 *bar*. A tensile force (F_p) is also applied on the reference node in the $z = L$ plane, equals to the applied internal pressure times the internal cross-section of the liner ($F_p = P_{in}\pi(D_l - 2t_l)^2/4$) in order to simulate the force at the two capped ends due to the pressure. This force will be referred to as "capped-end force", and remains constant during bending, following the orientation of reference node (follower force).

In the following results, the applied curvature (k) is normalized by the curvature-like parameter $k_l = t_o/d_{m,o}^2$ (where $d_{m,o}$ is the mean diameter of the outer pipe), so that $\kappa = k/k_l$; the bending moment M is normalized by $M_o = \sigma_{y,o}t_o d_{m,o}^2$, so that $m = M/M_o$; the detachment (Δ) of the liner pipe from the outer pipe is normalized by the liner thickness t_l, so that

$\Delta = (u_l - u_o)/t_l$, where u_l and u_o are the radial displacement of the liner and outer pipe, respectively at the most compressed generator of the pipe, as shown in Figure 4b. Furthermore, the ovalization (ζ) of the liner pipe cross-section is defined as $\zeta = (d_{h,l} - d_{v,l})/d_{m,l}$, where $d_{h,l}$ and $d_{v,l}$ is the deformed horizontal and vertical mean diameter of the liner, while $d_{m,l}$ is the initial mean diameter of the liner pipe. The local hoop curvature ($1/r_{\theta 0}$), hoop stress ($\sigma_{\theta 0}$) and axial stress (σ_{x0}) in the liner pipe are also computed at $\theta = 0$ (as shown in Figure 4b), where maximum compression occurs. The value of local curvature at $\theta = 0$ is associated with local buckling resistance of the cylinder. Finally, the local hoop curvature of the liner due to ovalization is normalized by $1/r_l$ and the longitudinal and hoop stresses on the liner are normalized by the yield stress of the liner $\sigma_{y,l}$.

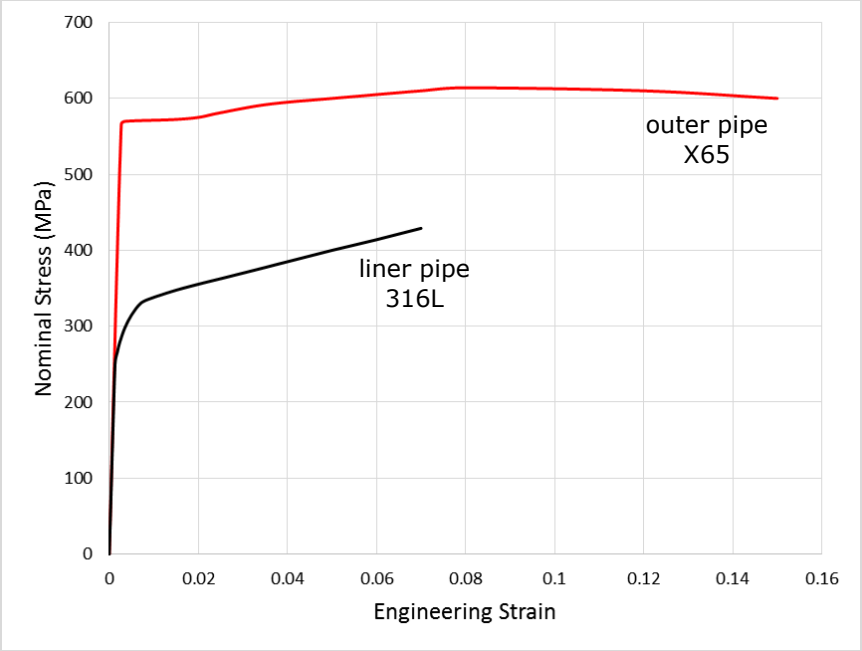

Figure 3: Stress-strain curves of outer and liner pipe.

3.1 OVALIZATION ANALYSIS

A quasi-two-dimensional (ovalization) analysis is conducted first, in order to understand some key features of lined pipe mechanical behaviour during bending in the presence of internal pressure. This analysis considers a lined pipe length equal to 3% of the diameter, as shown in Figures 2a,

2b. The detachment of liner from the outer pipe (Figure 4b) is presented in Figure 5, for TF Pipes (Figure 5a) and SF Pipes (Figure 5b). An important observation refers to the reduction of detachment size (amplitude) as the internal pressure increases. More specifically, in the case of $p = 10\%$, the detachment is practically zero, even for high values of applied curvature ($\kappa = 4$). The evolution of ovalization in SF and TF Pipes under bending for various levels of pressure is shown in Figure 6. The ovalization of the cross-section is slightly reduced with increasing internal pressure for high values of curvature. Furthermore, the results show that there is no difference between the response of SF Pipes and TF Pipes, which has also been observed by Vasilikis and Karamanos (2012) for non-pressurized lined pipes. Furthermore, Figure 7 shows the influence of different pressure levels on local hoop curvature of the liner pipe at the most compressed location of the cross-section $\theta = 0$ (Figure 4a). The results indicate that as the pressure level increases, the liner is more round. Furthermore, no difference is observed between SF and TF Pipes in terms of detachment and local hoop curvature.

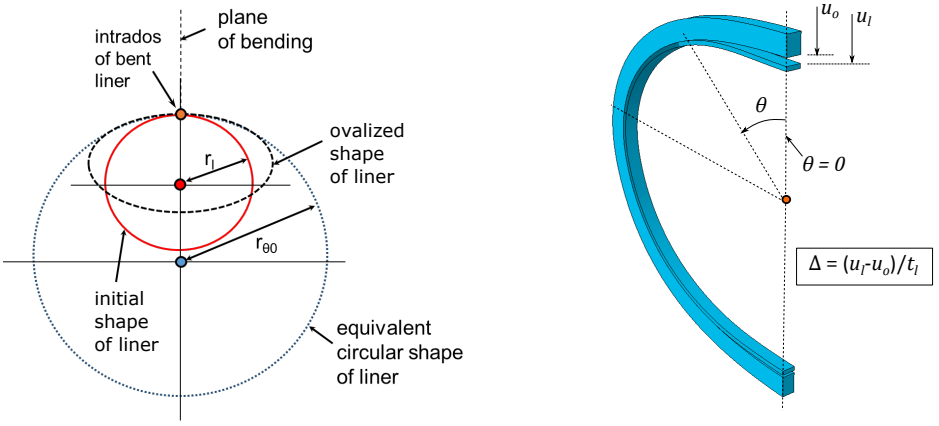

(a) (b)

Figure 4: (a) Schematic representation of liner ovalization and local radius of hoop curvature at the most compressed location ($\theta = 0$). (b) Liner detachment and cross-section ovalization.

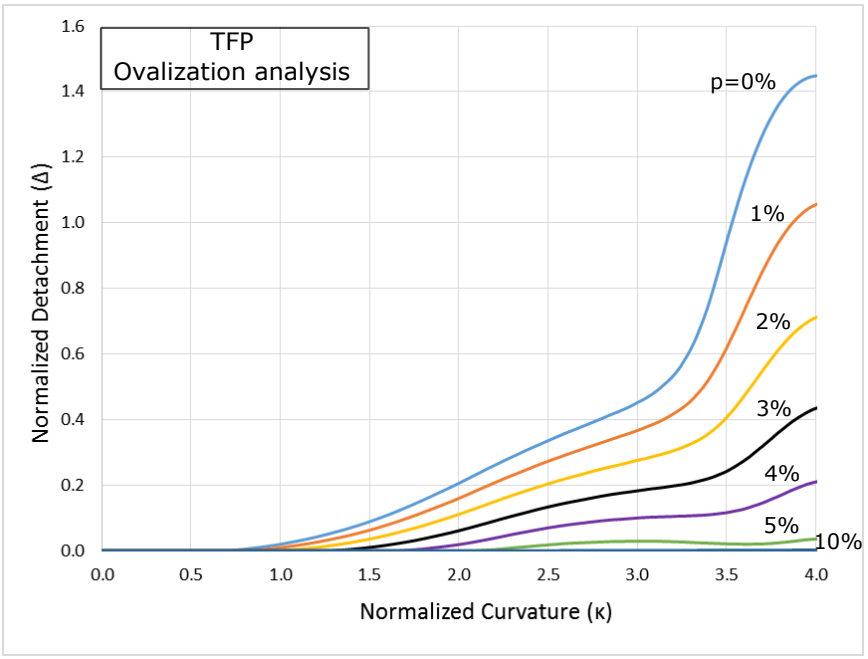

(a)

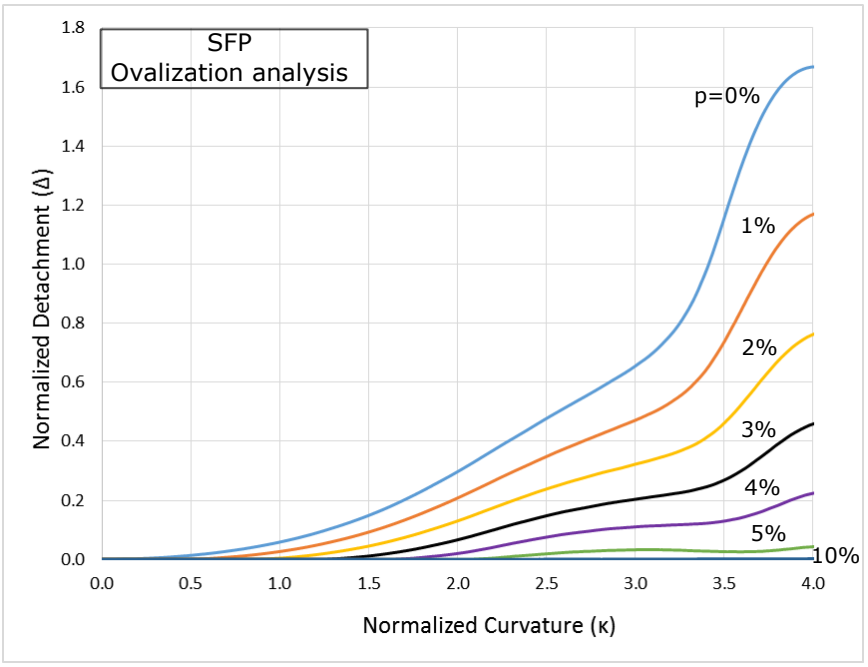

(b)

Figure 5: Detachment of liner from outer pipe for different levels of internal pressure (TF Pipe and SF Pipe); ovalization analysis.

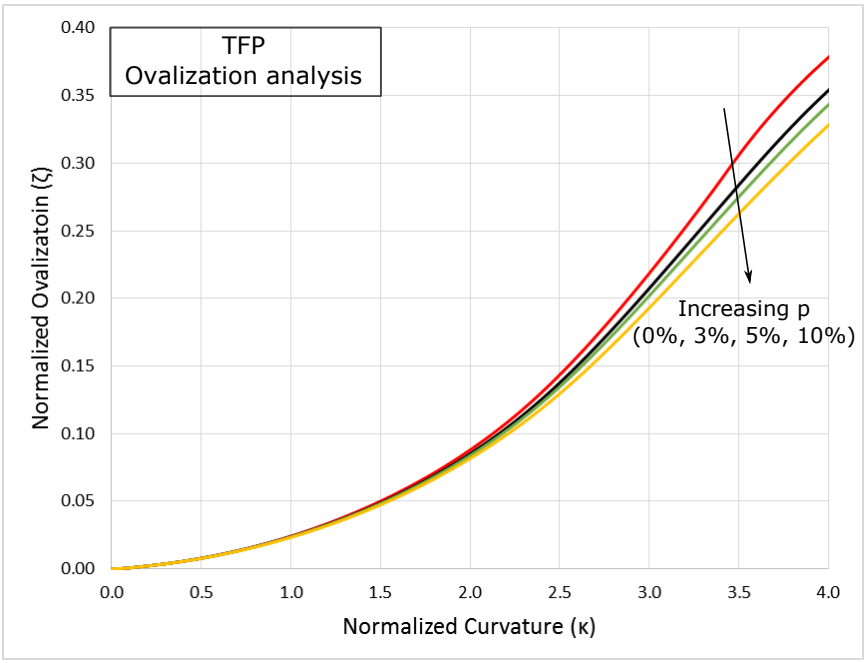

(a)

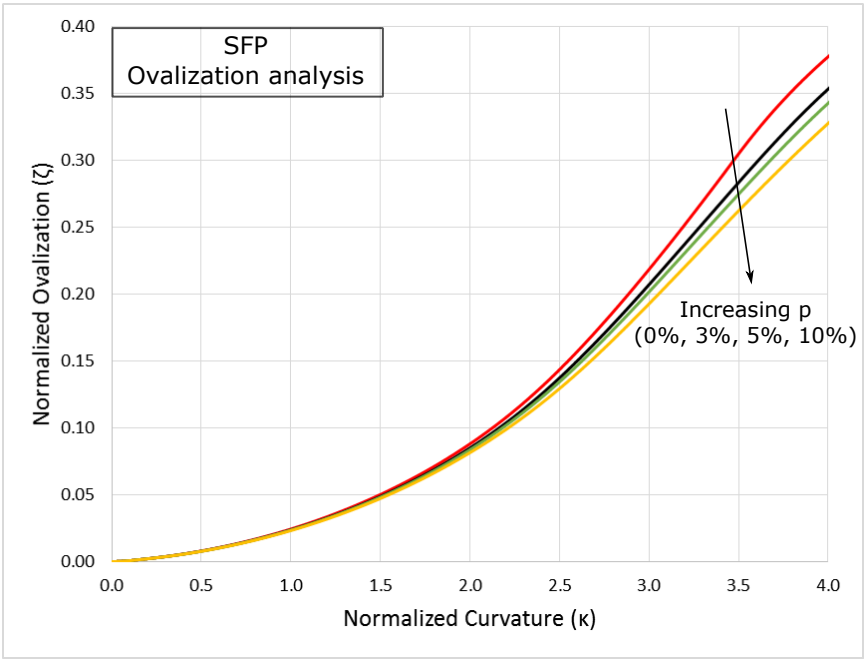

(b)

Figure 6: Increase of ovalization of liner cross-section in terms of applied curvature for different levels of internal pressure (TF Pipe and SF Pipe); ovalization analysis.

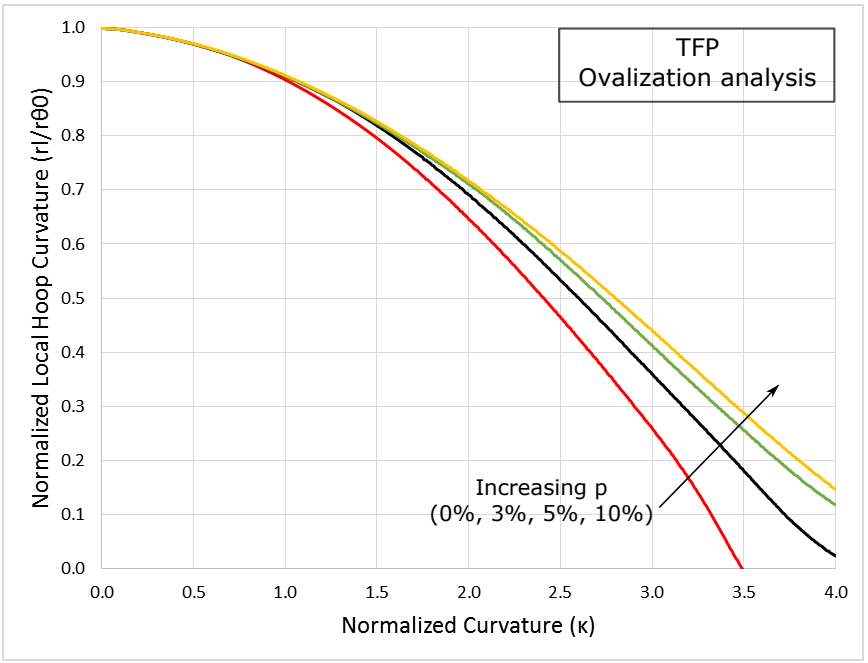

(a)

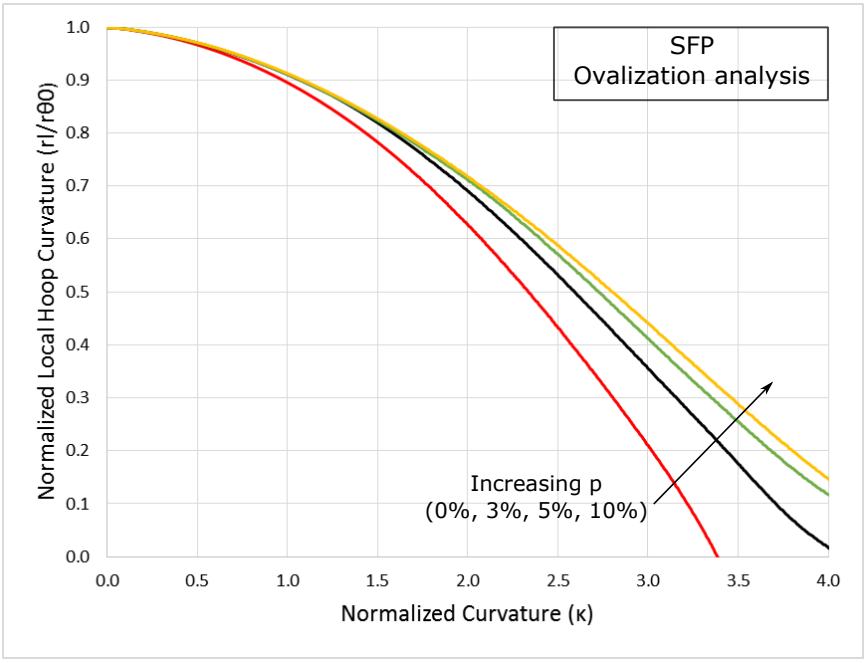

(b)

Figure 7: Evolution of local hoop curvature of liner at $\theta = 0$ in terms of applied curvature for different levels of internal pressure (TF Pipe and SF Pipe); ovalization analysis.

Figure 8 shows the influence of internal pressure on the evolution of average axial stress across the thickness at $\theta = 0$ on both SF and TF Pipe. This average stress is computed using Simpson integration over the wall thickness of the liner pipe. The abrupt drop of stress after a value of κ equal to about 3, is due to the severe cross-sectional ovalization of lined pipe. Figure 9 also shows the evolution of moment of the lined pipe for several levels of internal pressure. The results show that the applied moment decreases at normalized curvature κ values of about 3, which is also attributed to cross-sectional ovalization, which is interrelated with the corresponding decrease of axial stress of the liner pipe at $\theta = 0$, shown in Figure 8. Furthermore, Figure 10 presents the distribution of axial stress across the wall thickness of the liner for different values of normalized curvature. For small values of κ the distribution is quasi-constant (as shown in Figure 10), despite the fact that the liner material is already in the inelastic region, whereas the distribution for larger values of κ is influenced by exceed cross-sectional ovalization and local hoop bending. More specifically, hoop bending introduces hoop stresses that interact with longitudinal stresses due to inelastic material response through the von Mises yield criterion. Those hoop stresses are not constant across the thickness, and this results in a non-constant distribution of longitudinal stress as well. Figure 11 depicts the variation of average axial stress through liner thickness with respect to the distance from the neutral axis around the cross-section (y/r_l), for different values of curvature. For high values of curvature, this is a variation reminiscent of the corresponding variation of stress observed in curved pipes (elbows), as described in detail by Karamanos (2016). Figure 12 presents the hoop stress at $\theta = 0$ of liner during bending for the TF Pipe. In those diagrams, the hoop stresses are compressive, but are shown positive for the sake of convenience. In this case, the liner is pre-stressed, due to the manufacturing process and initial hoop stress is 55% of yield stress. Increasing the level of internal pressure, no difference on the detachment and local hoop curvature at $\theta = 0$ is observed between the response of SF and TF Pipes, even for high values of curvature, as indicated in Figures 13, 14. The values of detachment in Figure 13a are larger than those of Figure 13b by two orders of magnitude. Furthermore, the normalized local hoop curvature r_l/r_0 increases by approximately 160%, for $p = 10\%$ (Figure 14b) compared with non-pressurized pipes (Figure 14a), for high values of curvature. In the case of non-pressurized pipes the local

hoop curvature becomes zero at $\kappa = 3.5$, as shown in Figure 14a, indicating that the liner has become flat at $\theta = 0$ location; beyond that stage, the local hoop curvature becomes negative, indicating that "inversion" of the liner pipe wall has occurred.

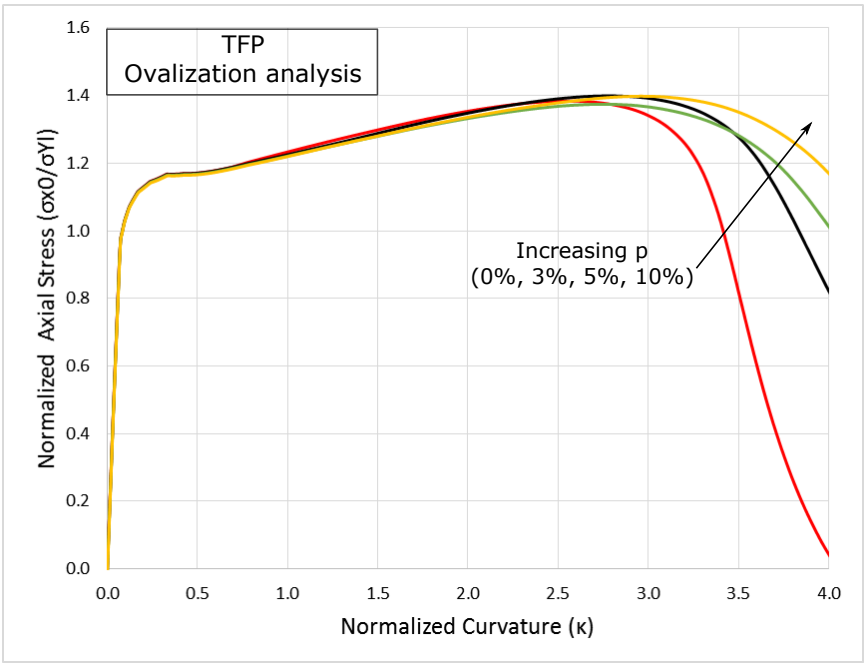

(a)

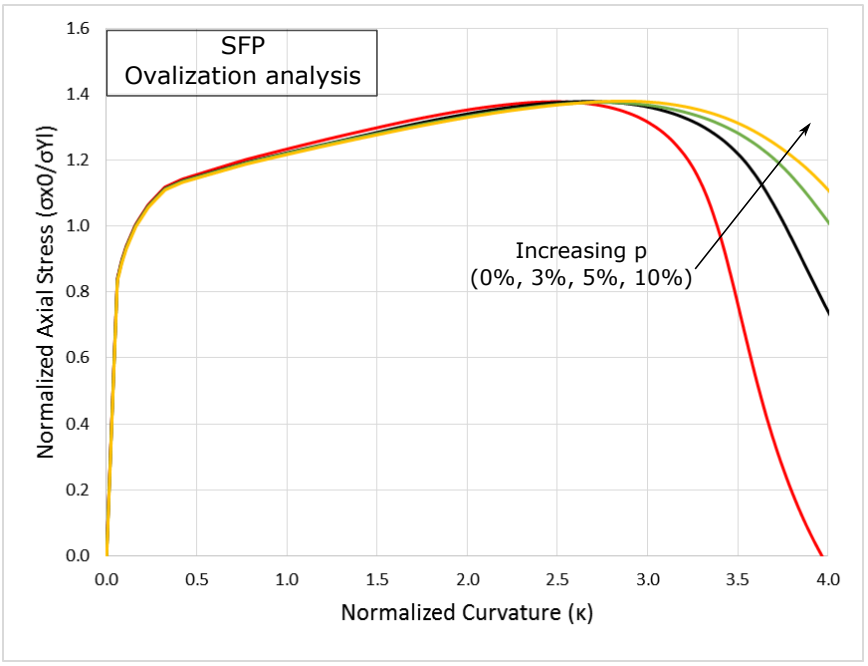

(b)

Figure 8: Evolution of average axial stress across the thickness of liner at $\theta = 0$ in terms of applied curvature for different levels of internal pressure (TF Pipe and SF Pipe); ovalization analysis.

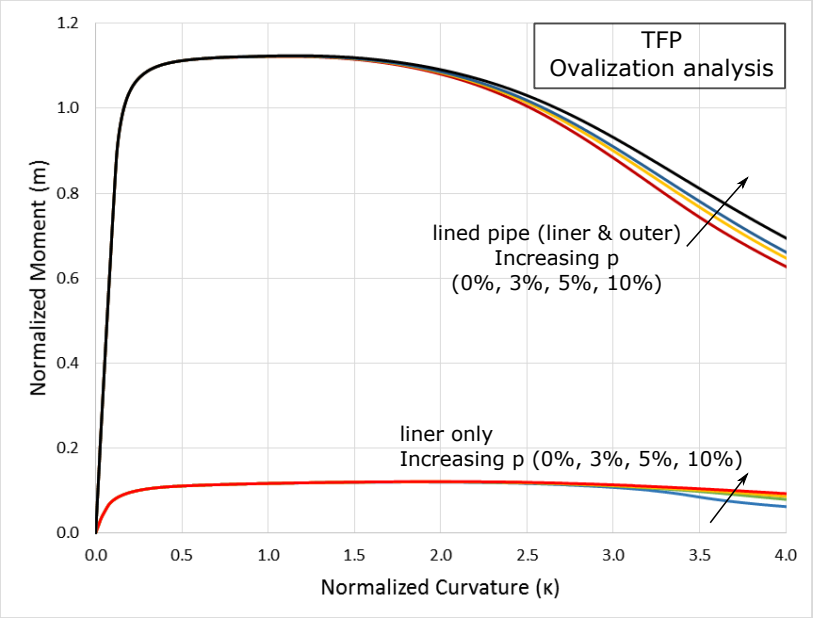

Figure 9: Bending moment for the entire lined pipe and for the liner only, in terms of applied curvature for different levels of internal pressure; ovalization analysis.

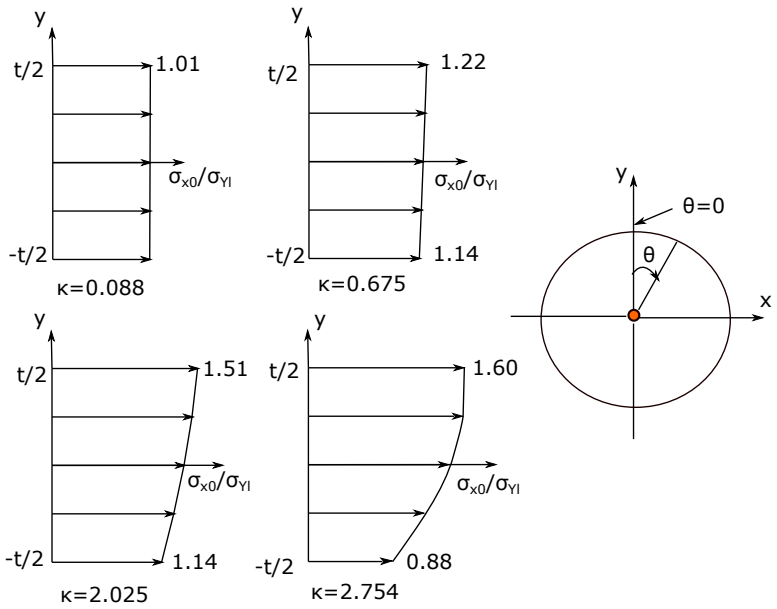

Figure 10: Variation of axial stress across the wall thickness at the most compressed location ($\theta = 0$) for different values of normalized curvature (κ); ovalization analysis.

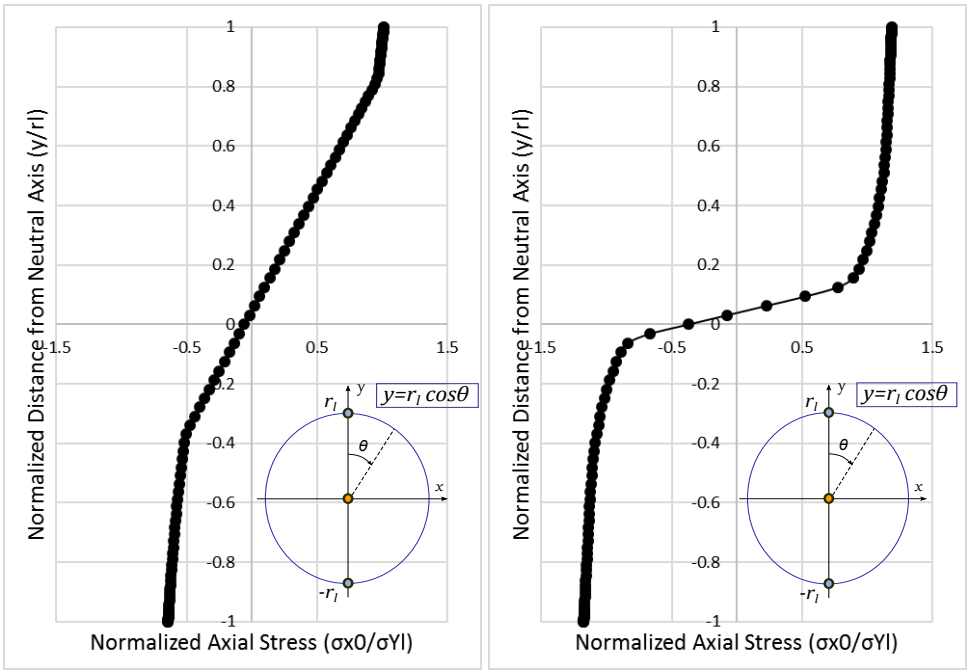

(a) $\kappa = 0.088$ (b) $\kappa = 2.025$

(c) $\kappa = 0.675$ (d) $\kappa = 2.754$

Figure 11: Variation of average axial stress around the cross-section of the liner pipe for different values of curvature (κ); ovalization analysis.

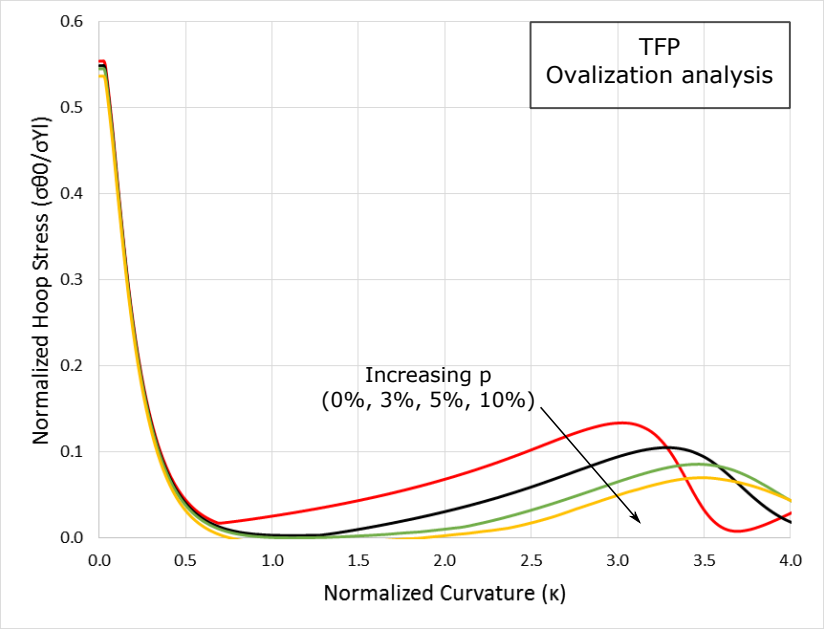

Figure 12: Variation of hoop stress in the liner pipe at $\theta = 0$, for different levels of internal pressure obtained from ovalization analysis (hoop stresses are compressive).

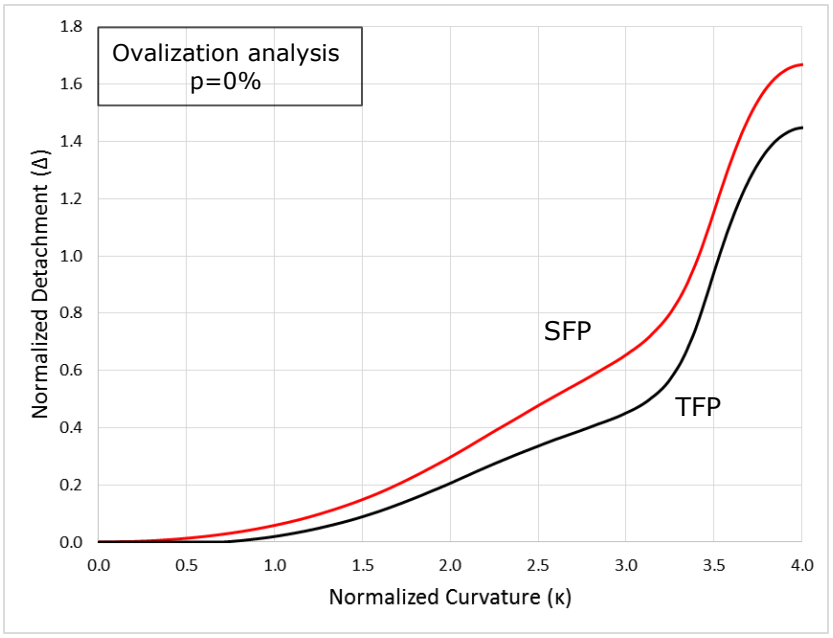

(a)

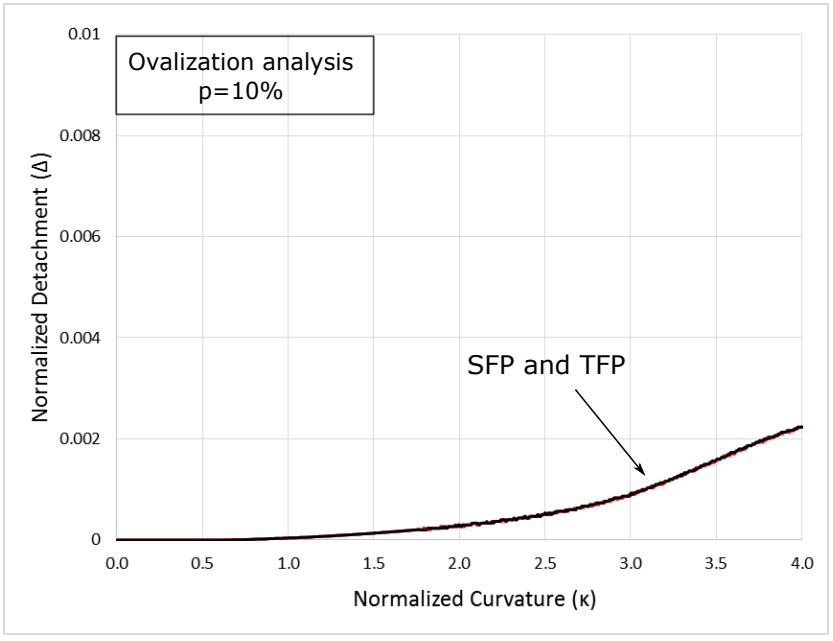

(b)

Figure 13: Comparison of liner detachment in SF and TF Pipes for $p = 0\%$ and $p = 10\%$; ovalization analysis.

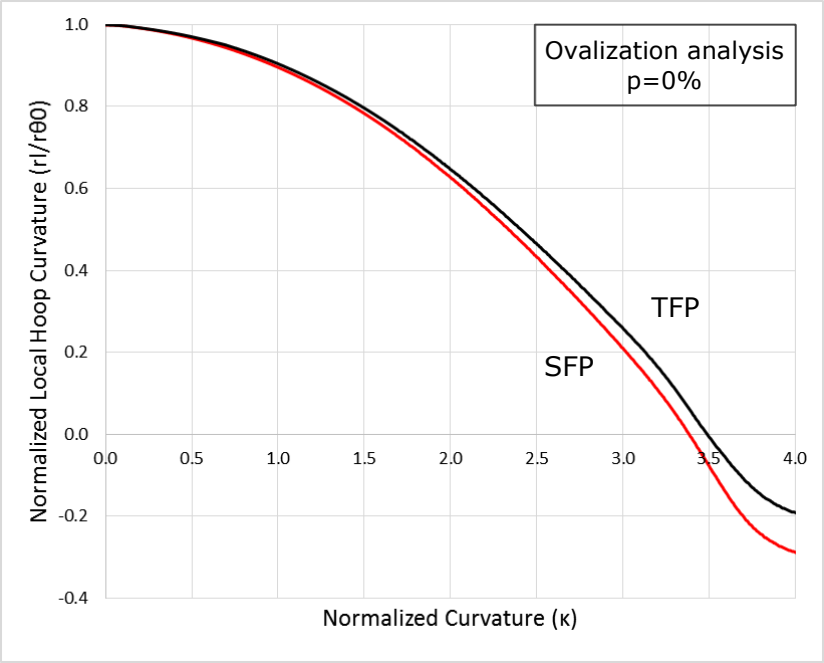

(a)

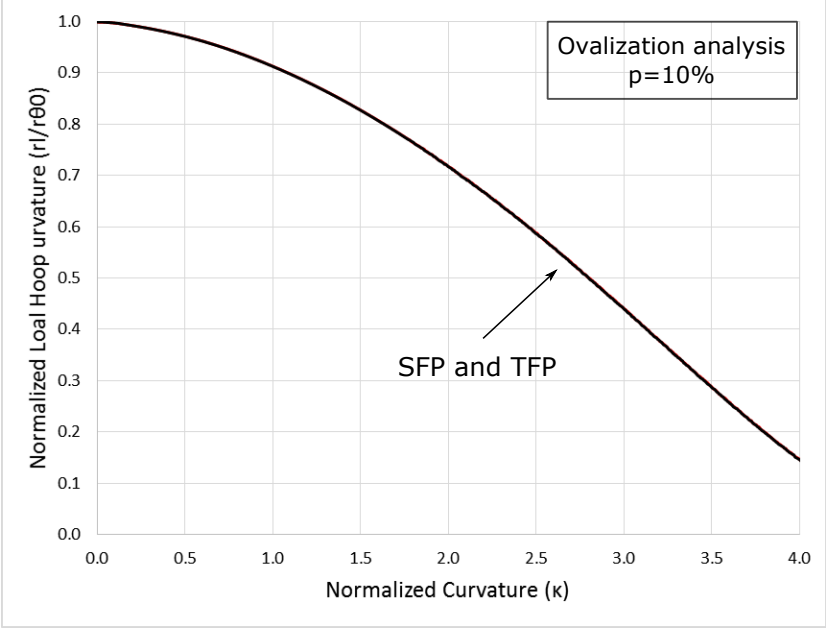

(b)

Figure 14: Comparison of normalized local hoop curvature at $\theta = 0$ between SF and TF Pipes, for $p = 0\%$ and $p = 10\%$; ovalization analysis.

3.2 BUCKLING ANALYSIS

The mechanical behaviour of internally-pressurized steel lined pipes in terms of local buckling is investigated using the three-dimensional model shown in Figures 2c, 2d, and the corresponding analysis will be referred to as "buckling analysis". The results in this section refer to imperfection-free liners, whereas the effect of initial imperfections on pressurized bending response is examined in the next section. Introducing the dimensionless length parameter $\chi = (L - z)/\sqrt{d_{m,l} t_l}$, the lined pipe normalized length is equal to 10, as shown in Figure 19a. Figures 15 to 18 show the gradual detachment of the liner with increasing curvature along the pipe at $\theta = 0$ for SF and TF Pipes respectively, for zero and 10% level of internal pressure. In those figures, the vertical axis depicts the normalized detachment (Δ), and the normalized length (χ) spans along the pipe, as shown in Figure 19a. In Figures 15 to 18, the normalized length is also shown in the symmetric part ($\chi = -10$ to $\chi = 0$) mirroring the numerical results for visualization purpose.

It is observed that, soon after bending loading is applied, the liner detaches from the outer pipe and a quasi-uniform wrinkling is formed along the pipe due to the outer pipe confinement at the compression side, as shown in Figure 20a. This detachment and uniform wrinkling has been identified by Vasilikis and Karamanos (2012) as a first bifurcation for the non-pressurized case, and is also apparent herein for the presence of low levels of internal pressure up to $p = 10\%$. A second bifurcation shown in Figure 21a occurs at higher curvatures, also observed by Vasilikis and Karamanos (2012). As the level of internal pressure increases, detachment of liner pipe occurs at a later stage, which is beneficial for the pipe, enabling the pipe to deform at higher values of applied curvature without exhibiting local buckling. In Figures 16 and 18 (referring to SF and TF Pipes respectively) much higher curvature values are noticed, compared with the corresponding values observed in the absence of internal pressure (Figures 15, 17). The results show that increasing the internal pressure, the uniformly wrinkled configuration (shown in Figure 20a) tends to vanish, in a way that local buckling occurs rather abruptly at a very localized pattern (Figure 20b). The deformed configuration for all cases of internal pressure of TF Pipe are presented in Figure 21 at normalized curvature $\kappa = 3$, showing clearly the influence of pressure on the local buckling shape. Increasing the level of pressure, a re-

duction of the height of the main buckle (A) and of the four adjacent minor buckles (B) (presented in Figure 19b) is observed, as shown in Figures 21 and 22.

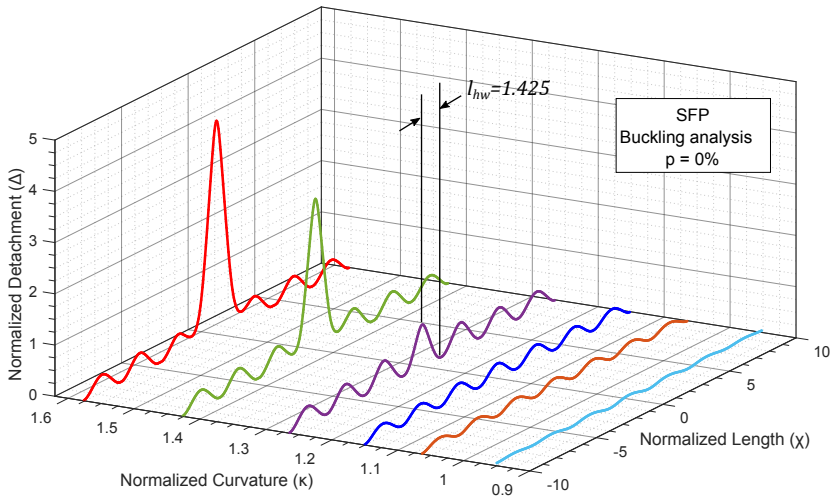

Figure 15: Normalized detachment at $\theta = 0$ along SF lined pipe under zero internal pressure.

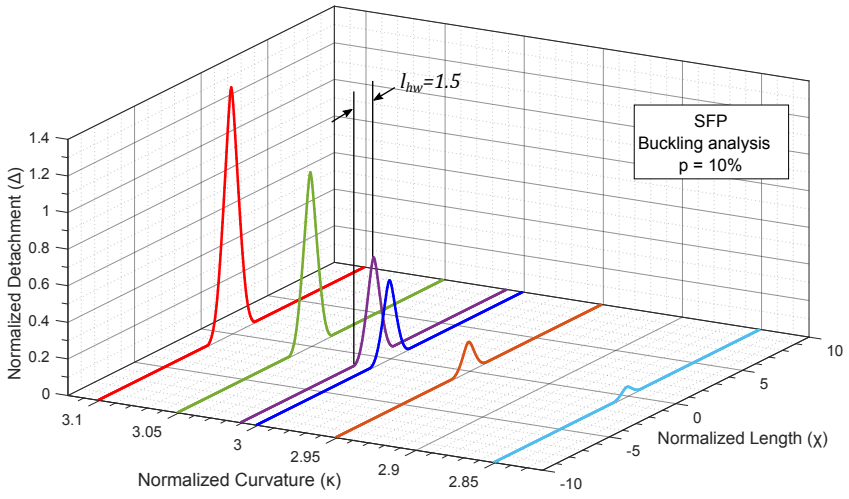

Figure 16: Normalized detachment at $\theta = 0$ along SF lined pipe under internal pressure $p = 10\%$.

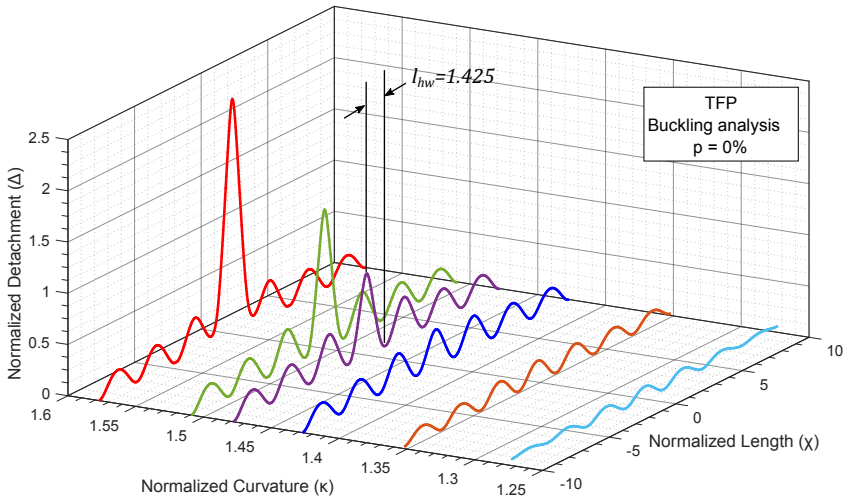

Figure 17: Normalized detachment at $\theta = 0$ along TF lined pipe under zero internal pressure.

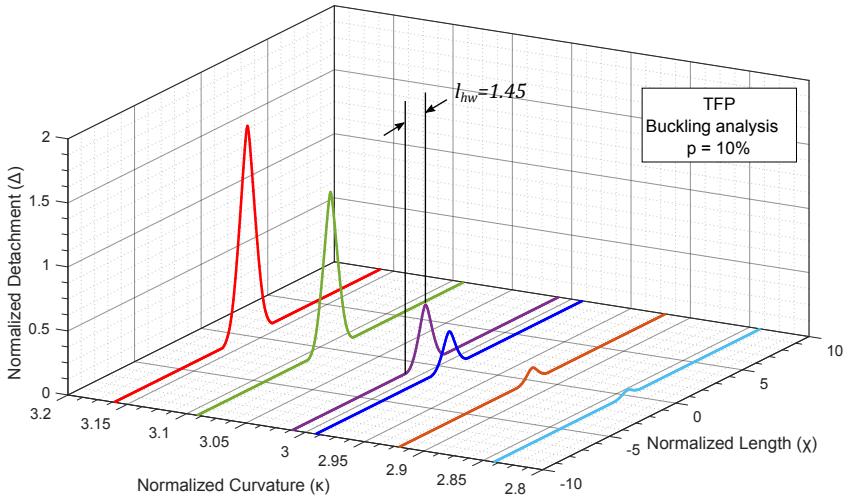

Figure 18: Normalized detachment at $\theta = 0$ along TF lined pipe under internal pressure $p = 10\%$.

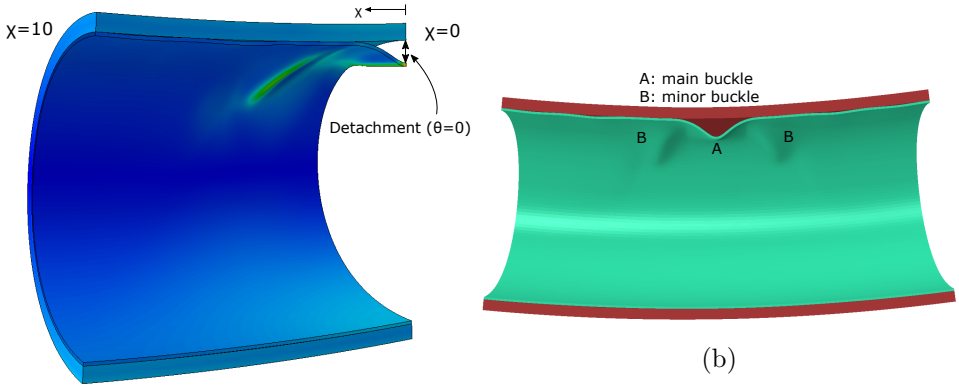

(a) (b)

Figure 19: (a) Liner pipe buckling shape at $\chi = 0$ location, (b) main buckle (A) and four adjacent minor buckles (B) of liner pipe.

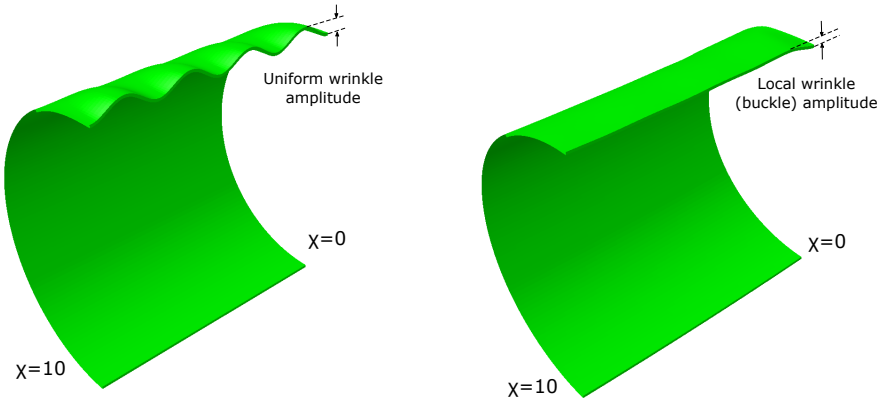

(a) (b)

Figure 20: (a) Uniform wrinkling of liner pipe (low pressure levels), (b) localized buckling pattern of liner pipe (higher pressure levels).

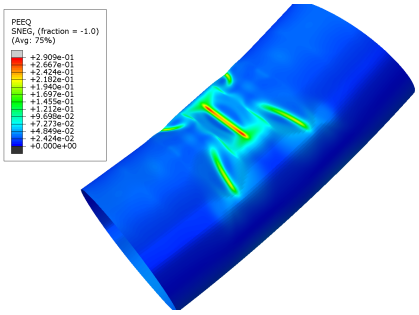

(a) $P_{in} = 0\%P_y$

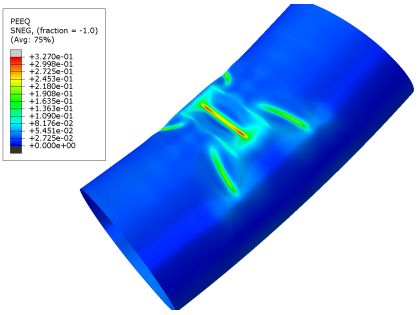

(b) $P_{in} = 1\%P_y$

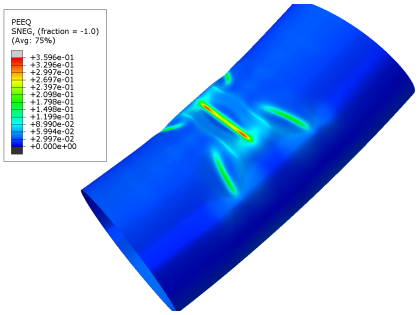

(c) $P_{in} = 2\%P_y$

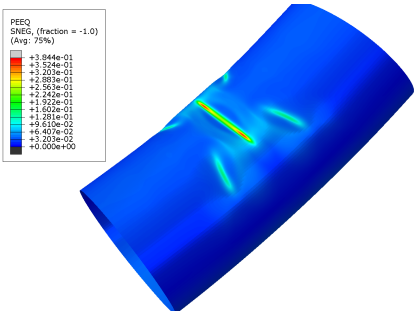

(d) $P_{in} = 3\%P_y$

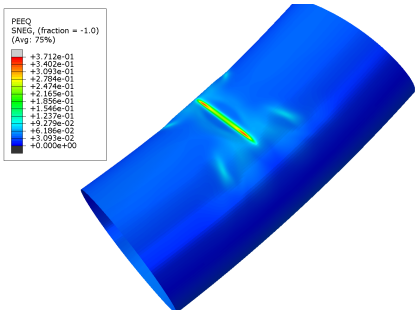

(e) $P_{in} = 4\%P_y$

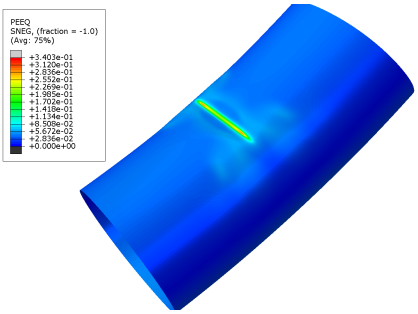

(f) $P_{in} = 5\%P_y$

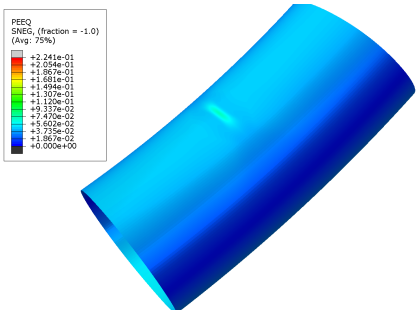

(g) $P_{in} = 10\%P_y$

Figure 21: Liner buckled configuration for a TF Pipe, showing the distribution of equivalent plastic strain at normalized curvature $\kappa = 3$, for different levels of internal pressure.

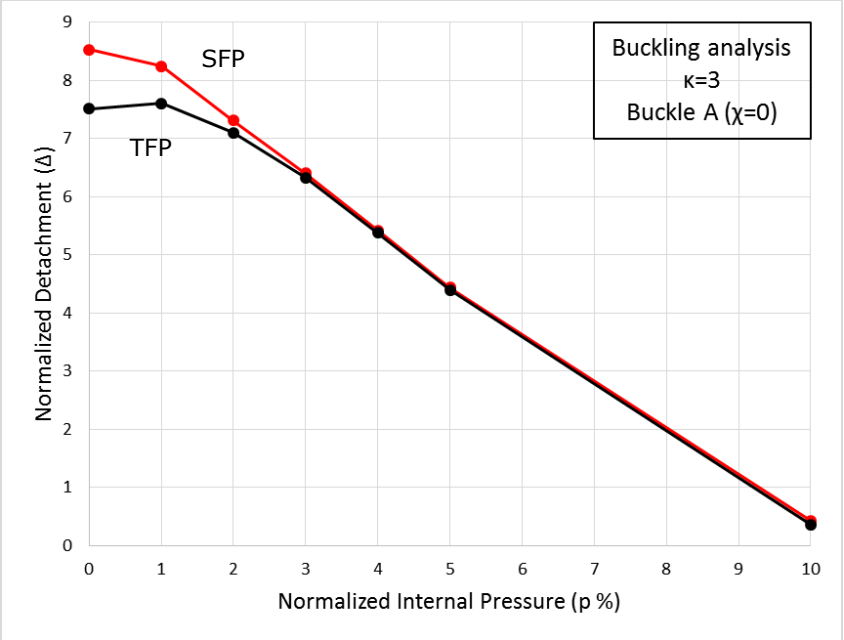

Figure 22: Normalized detachment (SF and TF Pipe) at main buckle (A) ($\chi = 0$) and curvature $\kappa = 3$ for different pressure levels.

At this point it is necessary to establish a definition of the "critical" curvature, so that a quantitative comparison of different cases is possible. The results in Figure 23a, for the case of zero internal pressure, show that the detachment increases rapidly beyond a specific value of curvature, resulting in the formation of local buckling of the liner pipe. In particular, there is a value of curvature, at which the gradient of detachment ($d\Delta/d\kappa$) reaches its maximum value, as shown in Figure 23b. For the purpose of our study, this value of κ is considered as the critical (buckling) curvature of the liner, denoted as κ_{cr}, so that beyond this curvature the liner pipe is considered structurally unstable.

The normalized half-wavelength ($l_{hw} = L_{hw}/\sqrt{d_{m,l}t_l}$) for non-pressurized SF and TF Pipes is equal to 1.425, as shown in Figures 15 and 17. These values are higher than the normalized half-wavelength of a single pipe exhibiting axisymmetric buckling, under axial compression and assuming elastic material behaviour (Timoshenko and Gere, 1961), which is equal to 1.222. This difference is attributed to both the lateral confinement of the liner pipe from the outer pipe and the inelastic behavior of the liner material. In the case of 10% internal pressure level, the half-wavelength (l_{hw}) of the localized buck-

ling pattern measured at the corresponding critical curvature value (κ_{cr}) is 1.5 and 1.45 for SF and TF Pipe, respectively (Figures 16, 18).

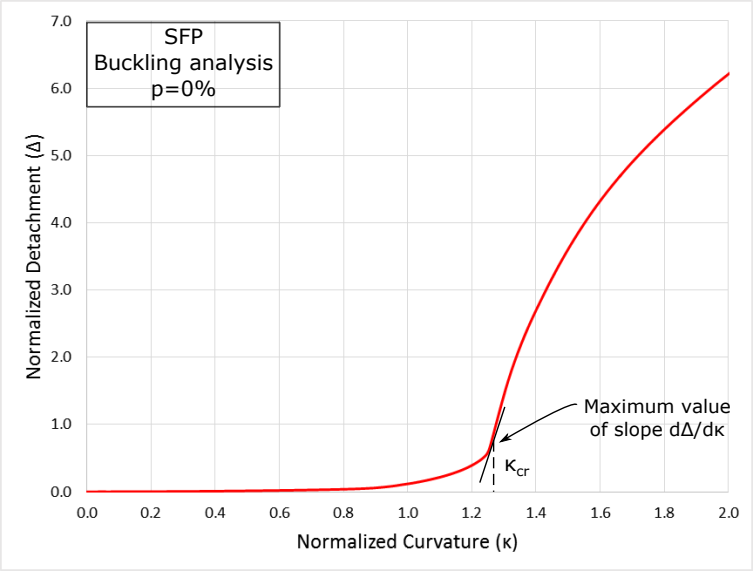

(a)

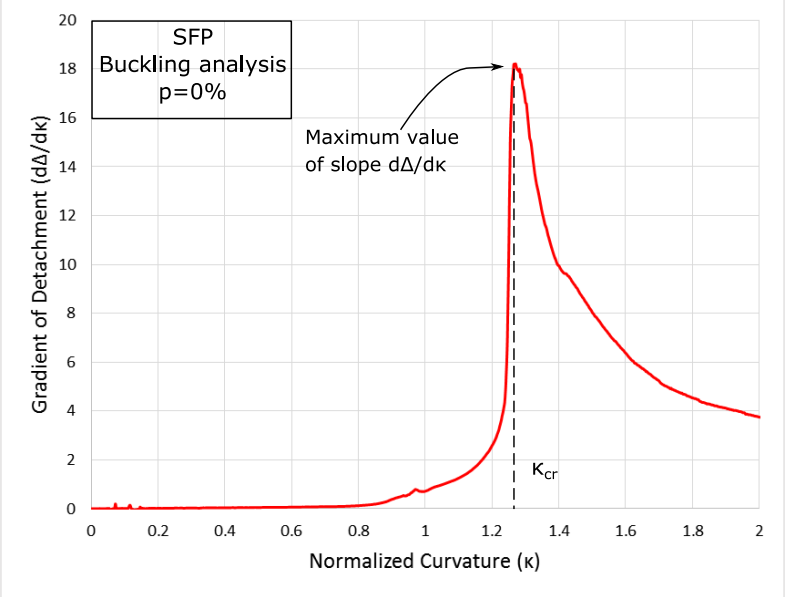

(b)

Figure 23: Variation of normalized detachment and gradient of detachment of SF Pipe without internal pressure, in terms of normalized curvature.

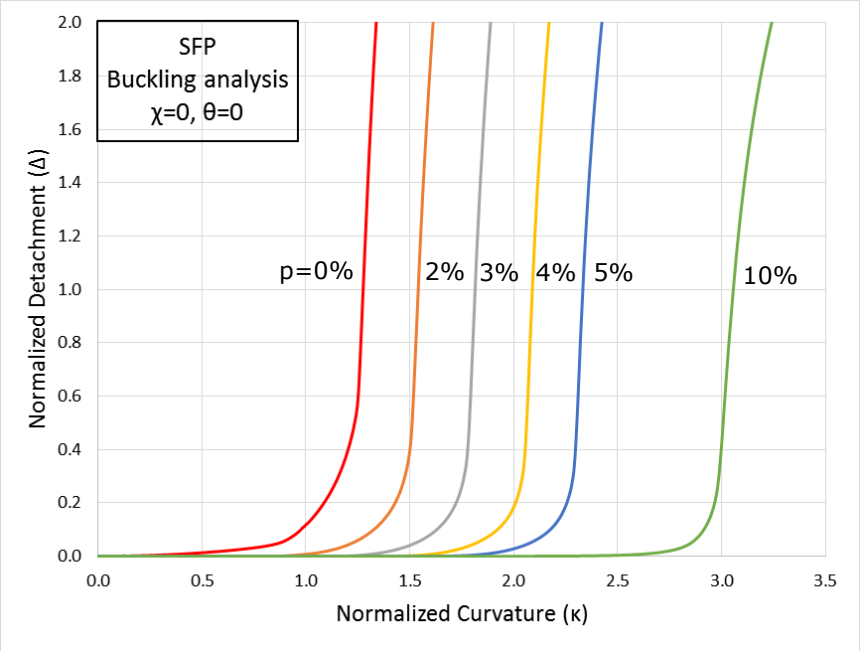

Figure 24: Normalized detachment at the center of the main buckle ($\chi = 0$ and $\theta = 0$) of SF Pipes for different levels of internal pressure.

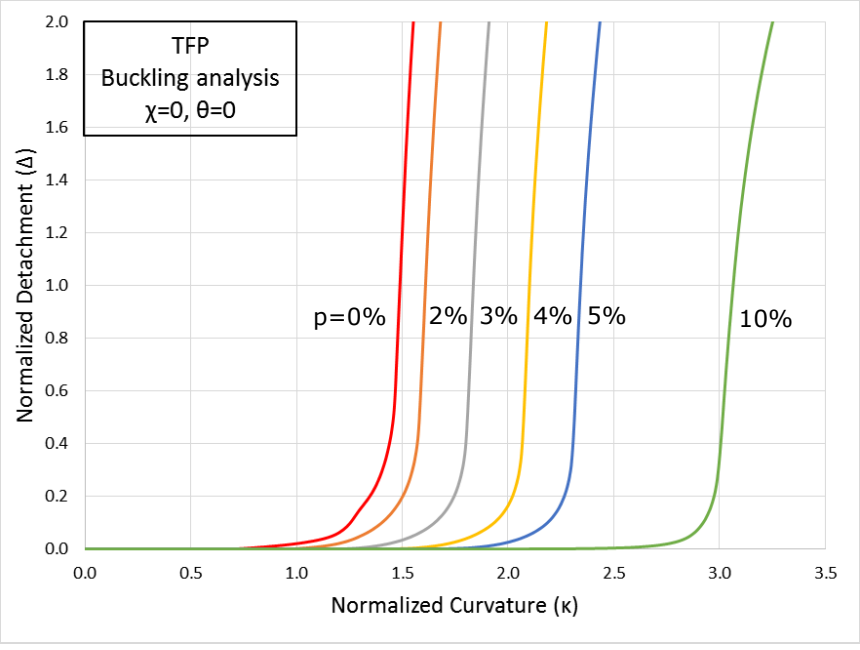

Figure 25: Normalized detachment at the center of the main buckle ($\chi = 0$ and $\theta = 0$) of TF Pipes for different levels of internal pressure.

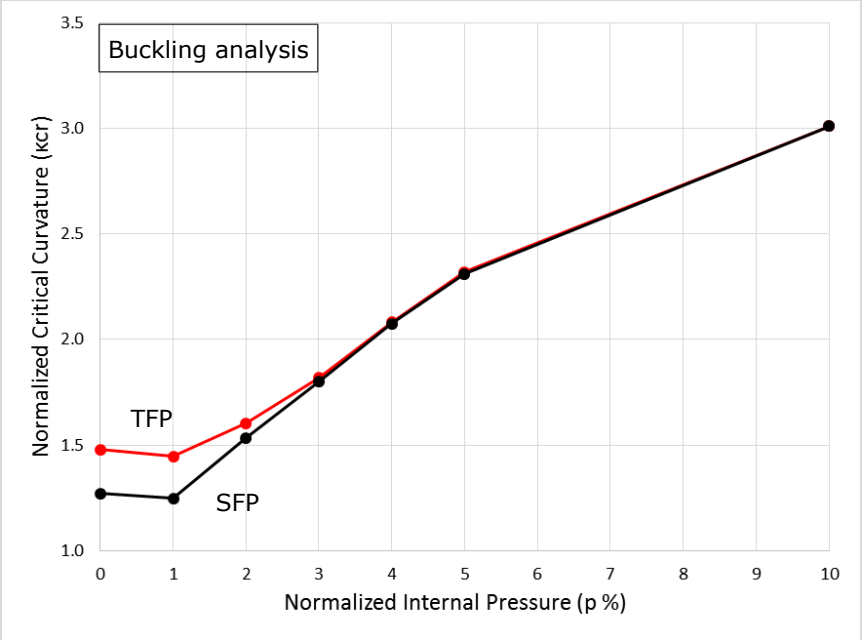

Figure 26: Normalized critical bending curvature κ_{cr} for the SF and TF Pipes with respect to the level of internal pressure.

Figures 24 and 25 show the beneficial role of internal pressure on bending response in terms of the value of the critical curvature κ_{cr} and the results are summarized in Table 1, including the values of the radius of curvature and the global bending strain (ϵ_b) for each type of pipe. In this Table the corresponding size of detachment (Δ_{cr}) for every level of internal pressure, for SF and TF Pipes respectively, is also shown. It is clear that κ_{cr} increases with increasing internal pressure. Additionally, Figure 26 presents the critical curvature for both types of pipe, with respect to the level of internal pressure, demonstrating the beneficial role of pressure. More specifically, the κ_{cr} value for the SF Pipe is increased by 138% in the case of 10% pressure level, compared with the κ_{cr} value at zero pressure. For the TF Pipe the corresponding increase is 104%. Also, as the internal pressure increases, the critical curvature (κ_{cr}) values for the two pipes become quite similar. In the case of 10% internal pressure level, the critical curvature values are practically identical for SFP and TFP.

Internal Pr. ($p\%$)	**Type of Pipe**	κ_{cr}	$\Delta_{cr}\%$	**Radius of curv.** (mm)	$\epsilon_b\%$
0	SFP	1.265	81.7	5337	2.96
	TFP	1.478	79.7	4567	3.44
1	SFP	1.248	78.9	5409	2.92
	TFP	1.445	75.8	4672	3.36
2	SFP	1.534	88.8	4401	3.56
	TFP	1.602	86.9	4214	3.71
3	SFP	1.800	73.5	3750	4.15
	TFP	1.818	67.4	3713	4.19
4	SFP	2.075	72.0	3253	4.76
	TFP	2.082	64.1	3242	4.77
5	SFP	2.310	61.0	2922	5.27
	TFP	2.320	61.3	2910	5.29
10	SFP	3.011	53.9	2242	6.76
	TFP	3.011	46.0	2242	6.76

Table 1: Critical curvature, corresponding normalized detachment, radius of curvature and global bending strain for different pressure values of SF and TF Pipes.

3.3 IMPERFECTION SENSITIVITY OF PRESSURIZED LINED PIPES

The numerical results for the critical curvature value κ_{cr}, shown in Table 1 for each level of internal pressure, refer to imperfection-free (perfect) pipes. In the present section sensitivity analysis of the bending response on the presence of initial imperfection is conducted for the case of 10% internal pressure level. The shape of initial imperfection for both SF and TF Pipe refers to the liner (the outer pipe has no imperfections) and is assumed in the form of the buckling configuration of the corresponding imperfection-free lined pipe and its amplitude, normalized by the liner pipe wall thickness (t_l), is denoted as Δ_0. It is expected that this shape of imperfection simulates the worst-case imperfection scenario for the liner pipe. It should be noted that other types of imperfection, such as mismatch of material properties between consecutive pipe segments, are not considered in the present study. As shown in Figures 16 and 18, the liner pipe at this level of pressure does

not exhibit uniform wrinkling, but, instead, it buckles locally with a main buckle, as shown in Figure 20b. The deformed configuration of the "perfect" pipe is imported as initial shape of the imperfect lined pipe and several imperfection amplitudes can be imposed through appropriate magnification. The initial imperfection amplitude Δ_0 ranges between 1% and 13.5% of the liner wall thickness t_l. It is noted though, that the wrinkled shape is imposed geometrically before initial pre-stressing is applied on the TF Pipe and prior to the application of internal pressure on both pipes. The influence of initial wrinkling imperfections on the bending response of both types of lined pipe is depicted in Figures 27, 28 ($p = 10\%$).

Furthermore, Figure 29 presents the critical curvature for both types of pipe with respect to the value of the imperfection amplitudes (Δ_0). With increasing imperfection amplitude, the critical curvature decreases, especially for SF Pipes. Furthermore, this imperfection sensitivity, for pressurized lined pipes, is significantly less pronounced for small values of Δ_0, compared to the one observed in the case of zero pressure as shown in Figure 29. The latter case has also been reported in the paper by Vasilikis and Karamanos (2012). The difference between SFP and TFP results is due to the effects of pre-stressing on the initial imperfection amplitude. Upon application of pre-stressing, the initial value of imperfection Δ_0 is significantly reduced to a lower value, which may referred to as "residual imperfection". The residual imperfection amplitude is significantly smaller compared to the Δ_0 value (as shown in Figure 30 and in Table 2). Furthermore, the presence of internal pressure further reduces the amplitude of this initial imperfection by a certain amount, also depicted in Figure 30 and Table 2. For initial imperfection of 10% amplitude, the κ_{cr} value decreases by 73% and 18% for SF and TF Pipe, respectively, with respect to the imperfection-free case. Table 3 summarizes the critical curvature κ_{cr}, with the corresponding value of detachment at buckling Δ_{cr}, in terms of the value of imperfection amplitude Δ_0.

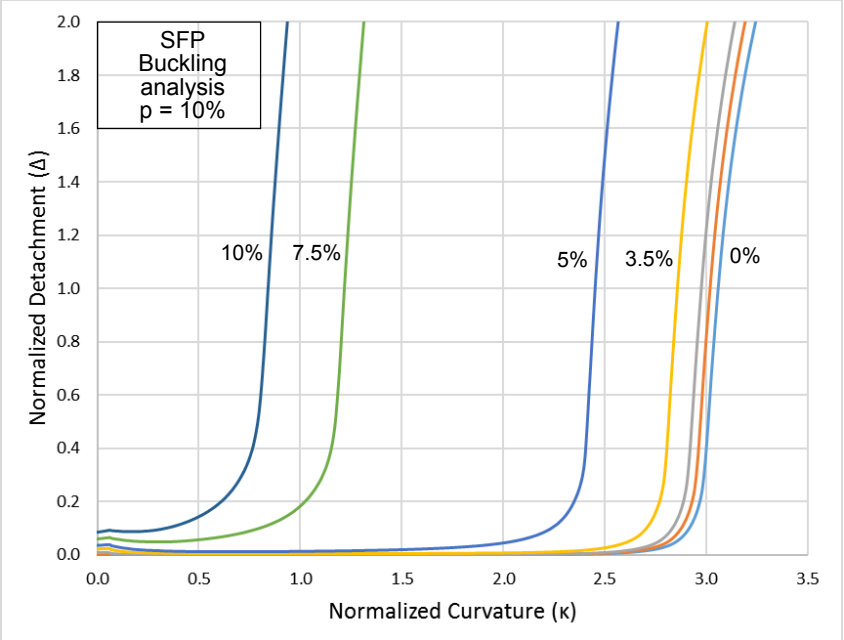

Figure 27: Development of liner detachment in SF Pipes with respect to applied curvature for different imperfection amplitudes ($p = 10\%$).

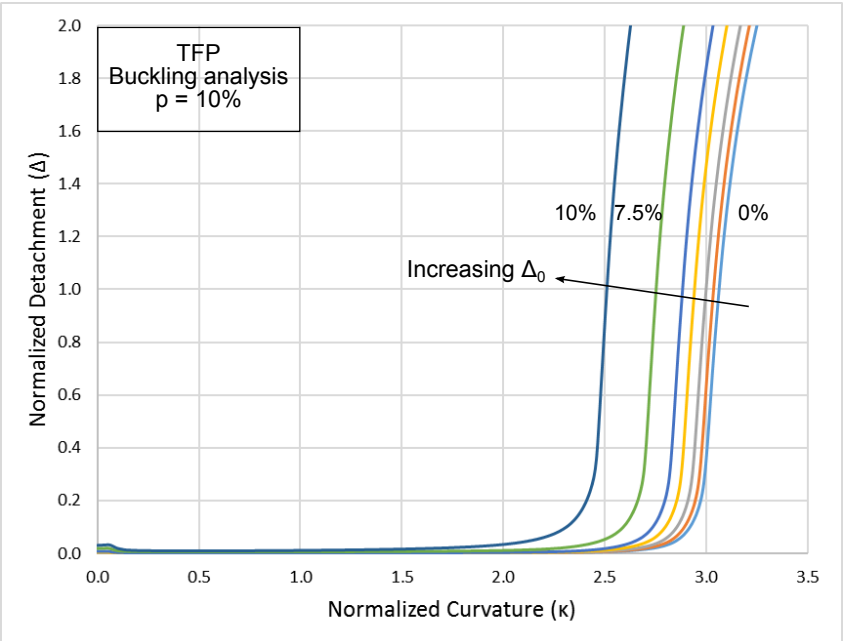

Figure 28: Development of liner detachment in TF Pipes with respect to applied curvature for different imperfection amplitudes ($p = 10\%$).

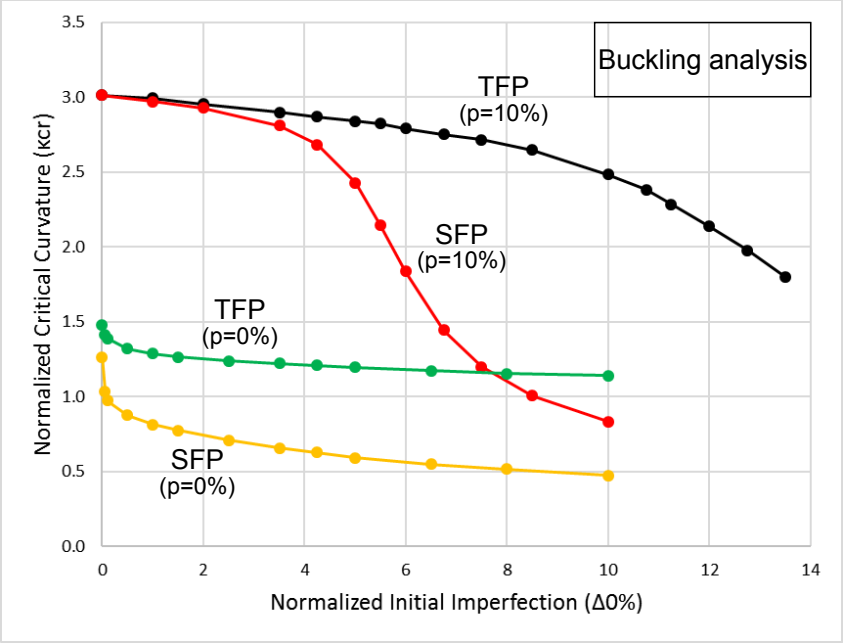

Figure 29: Variation of normalized value of critical curvature (κ_{cr}) of SF and TF Pipe in terms of initial imperfection amplitude ($p = 10\%$).

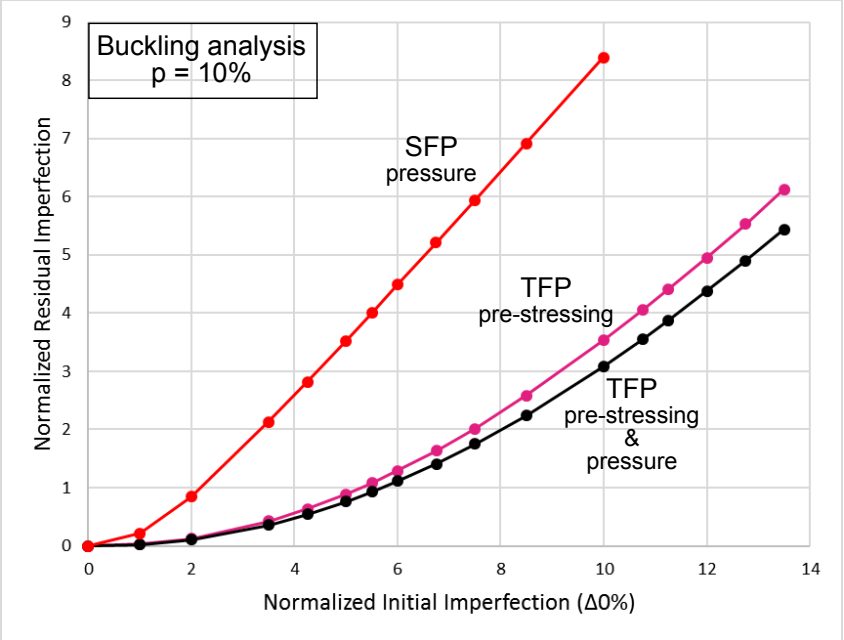

Figure 30: Normalized residual imperfection of SF and TF Pipes in terms of initial imperfection amplitude (Δ_0) for the case of $p = 10\%$.

Initial Imp. (Δ_0%)	**Residual Imp. of SFP**	**Residual Imp. of TFP**	
		After pre-stressing (before pressure)	**After pre-stressing and pressure**
1.0	0.216	0.027	0.024
2.0	0.845	0.124	0.106
3.5	2.131	0.421	0.358
4.25	2.820	0.635	0.542
5.0	3.528	0.888	0.764
5.5	4.006	1.076	0.931
6.0	4.487	1.287	1.111
6.75	5.212	1.637	1.409
7.5	5.991	2.016	1.749
8.5	6.919	2.584	2.240
10.0	8.394	3.537	3.087
10.75	-	4.058	3.547
11.25	-	4.411	3.873
12.0	-	4.954	4.381
12.75	-	5.528	4.905
13.5	-	6.125	5.436

Table 2: Residual imperfection amplitude in SF and TF Pipes with 10% internal pressure.

Initial Imp. ($\Delta_0\%$)	**Type of Pipe**	κ_{cr}	$\Delta_{cr}\%$
0	SFP	3.011	53.9
	TFP	3.011	46.0
1.0	SFP	2.971	51.8
	TFP	2.992	55.1
2.0	SFP	2.928	49.9
	TFP	2.953	51.8
3.5	SFP	2.810	45.8
	TFP	2.899	53.2
4.25	SFP	2.683	50.9
	TFP	2.868	49.8
5.0	SFP	2.428	69.0
	TFP	2.837	47.8
5.5	SFP	2.146	67.2
	TFP	2.822	56.0
6.0	SFP	1.836	76.7
	TFP	2.791	47.8
6.75	SFP	1.445	70.4
	TFP	2.752	49.0
7.5	SFP	1.199	77.4
	TFP	2.715	53.1
8.5	SFP	1.006	85.1
	TFP	2.647	60.8
10.0	SFP	0.832	88.1
	TFP	2.483	63.6
10.75	TFP	2.381	68.7
11.25	TFP	2.285	66.4
12.0	TFP	2.135	71.2
12.75	TFP	1.976	81.1
13.5	TFP	1.800	80.5

Table 3: Critical curvature and corresponding detachment for different imperfection amplitudes of SF and TF Pipes with 10% internal pressure level.

4 CONCLUSIONS

Using advanced numerical simulation tools, the mechanical behaviour of lined pipes, under monotonic bending has been examined in the presence of internal pressure up to 10% of nominal yield pressure ($P_y = 2\sigma_{y,l}t_l/d_{m,l}$). In the case of zero and low internal pressure levels (below 4% of P_y), the detachment of liner pipe from the outer pipe results in uniform wrinkling at the compression side followed by the formation of local buckling, characterized by a main buckle and four adjacent minor buckles. As the internal pressure level increases, the uniform wrinkling pattern vanishes and the lined pipe exhibits buckling quite suddenly in the form of a localized deformation pattern. A definition of critical curvature is also introduced, which allows for a consistent presentation of the numerical results. Increasing the internal pressure level, a significant increase on the critical curvature value κ_{cr} is observed. Additionally, the results show that the influence of liner pre-stressing due to manufacturing on the structural response of the lined pipe becomes smaller with increasing level of pressure. This influence disappears at a level of pressure equal to 10% of liner yield pressure. The results indicate that the presence of rather low-level of internal pressure may prevent liner buckling with beneficial effects on lined pipe installation process. Finally, the sensitivity of bending response on the presence of initial geometrical imperfections has been examined for internal pressure equal to 10% of the yield pressure of the liner for both SF and TF Pipes. It is found that the critical curvature of both types of lined pipe decreases for increasing imperfection amplitude, demonstrating that liner buckling in the presence of internal pressure is imperfection-sensitive, especially for SF Pipes. However this sensitivity, for small values of initial wrinkling amplitude is less pronounced compared to the non-pressurized case. It is shown that the residual imperfection is significantly affected by pre-stressing and plays a major role in the imperfection sensitivity of the liner.

ACKNOWLEDGEMENTS

The present work was supported by a Ph.D scholarship awarded to the first author from the School of Engineering, The University of Edinburgh, Scotland, UK.

References

Corona, E. and Kyriakides, S. (1988). On the collapse of inelastic tubes under combined bending and pressure. *International Journal of Solids and Structures*, **24(5): 505-535**.

Dama, E., Karamanos, S., and Gresnigt, A. (2007). Failure of locally buckled pipelines. *ASME, Journal of Pressure Vessel Technology*, **129(2): 272-279**.

Endal, G., Levold, E., and Ilstad, H. (2012). Method for laying a pipeline having an inner corrosion proof cladding. US Patent 8,226,327.

Focke, E.S. (2007). *Reeling of tight fit pipe*. Ph.D. thesis, Faculty of Civil Engineering, Delft University of Technology.

Hibbitt, H., Karlsson, B., and Sorensen, P. (2016). Abaqus analysis users manual version 2016. *Dassault Systèmes Simulia Corp, Providence*.

Hilberink, A. (2011). *Mechanical behaviour of lined pipe*. Ph.D. thesis, Faculty of Civil Engineering, Delft University of Technology.

Hilberink, A., Gresnigt, A., and Sluys, L. (2010*a*). A finite element method approach on liner wrinkling of snug fit lined pipe. In: *The Twentieth International Offshore and Polar Engineering Conference, Beijing, China*, International Society of Offshore and Polar Engineers.

Hilberink, A., Gresnigt, A., and Sluys, L. (2010*b*). Liner wrinkling of lined pipe under compression: a numerical and experimental investigation. In: *ASME 29th International Conference on Ocean, Offshore and Arctic Engineering, Shanghai, China*, American Society of Mechanical Engineers, OMAE2010-20285.

Hilberink, A., Gresnigt, A., and Sluys, L. (2011). Mechanical behaviour of lined pipe during bending: numerical and experimental results compared. In: *ASME 30th International Conference on Ocean, Offshore and Arctic Engineering, Rotterdam, The Netherlands*, American Society of Mechanical Engineers, OMAE2011-49434.

Howard, B. and Hoss, J.L. (2016). Method of spooling a bi-metallic pipe. US Patent App. 15/070,664.

Karamanos, S.A. (2016). Mechanical behavior of steel pipe bends: an overview. *ASME, Journal of Pressure Vessel Technology*, **138(4): 041203**.

Karamanos, S.A. and Tassoulas, J.L. (1991). Stability of inelastic tubes under external pressure and bending. *ASCE, Journal of Engineering Mechanics*, **117(23): 2845-2861**.

Kyriakides, S. and Corona, E. (2007). *Mechanics of offshore pipelines: volume 1 buckling and collapse*, volume 1. Elsevier.

Mair, J., Schuller, T., Holler, G., Henneicke, F., and Banse, J. (2013). Reeling and unreeling and internally clad pipeline. *US Patent Application Publication, US*, **34390**: p. A1.

Netto, T. and Estefen, S. (1994). Ultimate strength behaviour of submarine pipelines under external pressure and bending. *Journal of Constructional Steel Research*, **28(5): 137-151**.

Sriskandarajah, T., Roberts, G., Rao, V., *et al.* (2013). Fatigue aspects of cra lined pipe for hp/ht flowlines. In: *Offshore Technology Conference, Houston, Texas, USA*, Offshore Technology Conference, OTC 23932.

Timoshenko, S.P. and Gere, J.M. (1961). Theory of elastic stability. *McGrawHill-Kogakusha Ltd, Tokyo*, **109**.

Tkaczyk, T. and Pepin, A. (2014). Methods of reel-laying a mechanically lined pipe. US Patent 8,864,417.

Tkaczyk, T., Pepin, A., and Denniel, S. (2011). Integrity of mechanically lined pipes subjected to multi-cycle plastic bending. In: *ASME 30th International Conference on Ocean, Offshore and Arctic Engineering, Rotterdam, The Netherlands*, American Society of Mechanical Engineers, OMAE2011-49270.

Toguyeni, G.A., Banse, J., *et al.* (2012). Mechanically lined pipe: installation by reel-lay. In: *Offshore Technology Conference, Houston, Texas, USA*, Offshore Technology Conference, OTC 23096.

Vasilikis, D. and Karamanos, S.A. (2012). Mechanical behavior and wrinkling of lined pipes. *International Journal of Solids and Structures*, **49(23): 3432-3446**.

Vasilikis, D. and Karamanos, S.A. (2013). Wrinkling of lined steel pipes under bending. In: *ASME 32nd International Conference on Ocean, Offshore and Arctic Engineering, Nantes, France*, American Society of Mechanical Engineers, OMAE2013-11122.

Yuan, L. and Kyriakides, S. (2014*a*). Liner wrinkling and collapse of bi-material pipe under bending. *International Journal of Solids and Structures*, **51(3-4): 599-611**.

Yuan, L. and Kyriakides, S. (2014*b*). Plastic bifurcation buckling of lined pipe under bending. *European Journal of Mechanics-A/Solids*, **47: 288-297**.

Yuan, L. and Kyriakides, S. (2015). Liner wrinkling and collapse of girth-welded bi-material pipe under bending. *Applied Ocean Research*, **50: 209-216**.